Applied Catalysis B: Environmental 176–177 (2015) 522–531

Contents lists available at ScienceDirect

Applied Catalysis B: Environmental

journal homepage: www.elsevier.com/locate/apcatb

Stepwise tuning of metal-oxide and acid sites of CuZnZr-MFI hybrid catalysts for the direct DME synthesis by CO_2 hydrogenation

F. Frusteri [a], G. Bonura [a,*], C. Cannilla [a], G. Drago Ferrante [a], A. Aloise [b], E. Catizzone [b], M. Migliori [b], G. Giordano [b]

[a] CNR-ITAE, Istituto di Tecnologie Avanzate per l'Energia "Nicola Giordano", Via S. Lucia sopra Contesse, 5, 98126 Messina, Italy
[b] Università della Calabria, Dip. Ingegneria per l'Ambiente e il Territorio ed Ingegneria Chimica, Via P. Bucci (Cubo 44a), 87036 Arcavacata di Rende, CS, Italy

ARTICLE INFO

Article history:
Received 11 February 2015
Received in revised form 8 April 2015
Accepted 16 April 2015
Available online 17 April 2015

Keywords:
CO_2 hydrogenation
Dimethyl ether
Cu–ZnO–ZrO_2 catalysts
Zeolites

ABSTRACT

Multifunctional CuZnZr-zeolite catalysts were investigated for the direct synthesis of dimethyl ether (DME) from carbon dioxide (CO_2) hydrogenation. Physical mixtures prepared by pre-pelletized CuZnZr methanol catalysts and home-made MFI-type zeolites as well as hybrid systems prepared by coprecipitation of metal-oxide precursors in solutions containing the zeolites were tested in a plug-flow reactor at 240 °C, pressure of 3.0–5.0 MPa and space velocity comprised between 2500 and 10,000 $NL/kg_{cat}/h$. Preliminary experiments in methanol (MeOH) synthesis reaction from CO_2–H_2 mixtures allowed to individuate a suitable CuZnZr composition ensuring good activity in CO_2 conversion, high MeOH selectivity and limited CO formation. Parallel tests in MeOH-to-DME reaction were also carried out to investigate the functionality of the zeolites prepared. The results disclosed that an optimal Si/Al ratio is necessary to obtain dehydration catalysts characterized by suitable acidity and good resistance to deactivation in presence of water. The performance of the multifunctional CuZnZr-MFI catalysts in the direct CO_2-to-DME hydrogenation reaction showed that, by controlling the coprecipitation of CuZnZr methanol synthesis precursors, the availability of the active sites is maximized over the zeolite surface. That allowed to reach both high CO_2 conversion levels (up to 24%) and high rate of MeOH dehydration to DME.

1. Introduction

The development of green substitutes to fossil fuels has become an important task for energy and environmental sustainability. A good solution is chemical recycling and utilization of CO_2 to produce renewable, carbon neutral fuels, like methanol (MeOH) or dimethyl ether (DME) [1–4]. In particular, DME is a potential alternative fuel to diesel used in compression ignition engines [5,6]. This is due to its higher cetane number (55–60) and lower auto-ignition temperature (235 °C) in respect of diesel fuel (40–50 and 250 °C) [7]. The physical properties of DME are similar to those of liquefied petroleum gas (LPG) [8]; therefore, DME can also be used as a LPG substitute for household and industrial purposes. Other advantages of DME utilization as a fuel or feedstock include: (i) higher oxygen content and lower boiling point; (ii) less air pollutants emissions from its burning; (iii) more efficient reforming for hydrogen production; (iv) lower risk in damaging health during its usage [9].

Conventionally DME can be obtained in a two-step process [10–12] or in a single step (direct) process [13,14]. In the two step process, methanol is generally synthesized from syngas (CO–H_2 mixtures) on a metal-oxide catalyst in the first step. However, the utilization of CO_2, as an alternative feedstock instead of CO, is considered a more effective way for methanol production [15,16]:

$$CO_2 + 3H_2 \leftrightarrows CH_3OH + H_2O \quad (\Delta H^0 = -49.4\,kJ\,mol^{-1}) \tag{1}$$

Subsequently, DME is produced through methanol dehydration/condensation on an acid catalyst in the second step:

$$2CH_3OH \leftrightarrows CH_3OCH_3 + H_2O \quad (\Delta H^0 = -23.4\,kJ\,mol^{-1}) \tag{2}$$

In addition to the Reactions (1) and (2), the DME synthesis is also affected by the reverse water gas shift (RWGS) reaction:

$$CO_2 + H_2 \leftrightarrows CO + H_2O \quad (\Delta H^0 = +41.2\,kJ\,mol^{-1}) \tag{3}$$

and by the decomposition of methanol to CO:

$$CH_3OH \leftrightarrows CO + 2H_2 \quad (\Delta H^0 = +90.6\,kJ\,mol^{-1}) \tag{4}$$

* Corresponding author. Tel.: +39 090 624 205.
E-mail address: giuseppe.bonura@itae.cnr.it (G. Bonura).

http://dx.doi.org/10.1016/j.apcatb.2015.04.032
0926-3373/

From a thermodynamic point of view, a decrease in reaction temperature or an increase in reaction pressure could favor the synthesis of methanol. However, from a kinetic point of view an increase of reaction temperature above 240 °C facilitates the CO_2 activation rate and the formation of methanol or carbon monoxide [15,17]. Therefore, a highly selective catalyst is required to avoid the formation of undesired by-products [17,18].

In recent years, the feasibility of a single step process for the production of DME from CO_2–H_2 mixtures is attracting a research interest increasingly growing, because of lower thermodynamic limitation and increasing economic benefits, from reduced investment and operational costs [2,19–22]. In the direct CO_2 hydrogenation process, the net reaction is given by:

$$2CO_2 + 6H_2 \leftrightarrows CH_3OCH_3 + 3H_2O \quad (\Delta H^0 = -122.2\,kJ\,mol^{-1}) \qquad (5)$$

Also in this case, promoted by the carbon dioxide presence, the RWGS Reaction (3) can take place as parallel reaction. In order to maximize the DME productivity, the design of multifunctional/hybrid catalysts characterized by highly specific active sites is fundamental [23–26]. Generally, after methanol is generated over a metal-oxide catalyst functionality, it is immediately dehydrated over a neighboring acidic site, thereby enhancing the forward reaction and limiting the CO_2 consumption via-RWGS reaction [17,25–29]. Therefore, the direct catalytic hydrogenation of CO_2 into DME is typically performed in presence of physical/mechanical mixtures between a Cu-based methanol synthesis catalyst (usually, CuO–ZnO–Al_2O_3 or CuO–ZnO–ZrO_2) [2,17,19,22,25,26,28,30–36] and a solid acid catalyst, such as γ-Al_2O_3, silica–alumina (less or more modified) or different types of zeolites [17,28,37–40], responsible for methanol dehydration.

In this paper, a step by step optimization of the catalyst design for direct synthesis of DME from CO_2–H_2 mixtures will be described, starting from the investigation of the suitable composition of a CuO–ZnO–ZrO_2 catalyst for the CO_2-to-MeOH hydrogenation reaction, followed by the fine-tuning of the Si/Al ratio of a home-made MFI-type HZSM-5 zeolite for MeOH-to-DME dehydration reaction. Although the use of zeolites in the studied reaction does not allow to exploit their typical potential of shape/size selectivity owing to the small size of the involved molecules, however zeolites are also characterized by other important features, such as tunable solid acidity, high surface area, microporosity or loading property, representing the fundamental reasons why these unique structures are utilized as carriers of metals and/or metal-oxides. At the end, the process productivity of a physical mixture between the selected CuZnZr methanol catalyst and zeolite (at different extent of mixing) will be assessed in the direct CO_2-to-DME hydrogenation reaction and compared with the performance of a multifunctional system, in which the two methanol-synthesis and methanol-dehydration functionalities have been locally "integrated" during gel-oxalate precipitation of the Cu-Zn-Zr precursors in a solution containing zeolite particles finely dispersed, providing useful insights for future industrial applications of such multi-site catalysts.

2. Experimental

2.1. Catalysts for CO_2-to-MeOH synthesis

Three Cu–Zn–Zr catalysts at different composition, with a Cu loading ranging from 33 to 60 at. %, were prepared according to the gel oxalate coprecipitation method [41]. $Cu(NO_3)_2{\cdot}2{,}5H_2O$, $Zn(NO_3)_2{\cdot}6H_2O$ and $ZrO(NO_3)_2{\cdot}nH_2O$ were solubilized in ethanol and coprecipitated by oxalic acid at room temperature under vigorous stirring. The precipitates were dried at 110 °C for 16 h and then calcined at 350 °C for 4 h.

2.2. Zeolites for MeOH-to-DME dehydration reaction

Four MFI-type HZSM-5 zeolites were prepared starting from the following molar composition:

$$0.1Na_2O - 0.08TPABr - 1SiO_2 - xAl_2O_3 - 20H_2O$$

with $0.005 < x < 0.033$, where the alumina amount was varied according to the expected Si/Al molar ratio: 15, 25, 50 and 100. The synthesis gel was prepared following a method detailed elsewhere [42]: 2.66 g of sodium hydroxide (Aldrich) was added to 119.40 mL of distilled water. The appropriate amount of aluminum hydroxide (Aldrich) was solubilized into the basic solution and 7.10 g of tetrapropylammonium hydroxide (Aldrich) were then added to the gel. As last step, the addition of 19.95 g of precipitated silica (Merck) in the batch was followed by stirring (2 h) at room temperature. The crystallization was carried out in 150 mL PTFE-lined stainless steel autoclave in static conditions at 175 °C. After 96 h of crystallization, the solid phase was separated from the liquid by filtration, washed several times with distilled water and dried at 100 °C overnight. In order to give the acidic properties to the catalyst, the samples were calcined at 550 °C for 8 h and a double proton exchange procedure was performed by using 100 mL per catalyst gram of aqueous solution 1 M of NH_4Cl refluxed at 80 °C. The ammonia was then eliminated by calcination, obtaining the final H-MFI form at different Si/Al ratios.

2.3. Hybrid systems for one-step CO_2-to-DME hydrogenation reaction

The preparation procedure of the hybrid systems consists in the combination of the methanol catalyst with the zeolite. Preliminarily, two "homogeneous" physical mixtures constituted by a pre-synthesized methanol synthesis catalyst and a selected zeolite were realized, with a weight ratio of 1:1 and 9:1, respectively. Besides, in the attempt to chemically combine the catalytic functionalities necessary for the direct CO_2-to-DME hydrogenation reaction, so that the two parent catalysts were not distinguishable anymore, the generation of the methanol CuZnZr catalyst was directly performed in a solution containing the zeolite finely dispersed (particle size < 100 μm). So, during the gel-oxalate coprecipitation of the metal precursors, the zeolite was "englobed" in a system containing both metal-oxide sites (characteristic of methanol catalyst) and acid sites (typical of H-MFI zeolite). The solution of metal precursors was added, at room temperature and in a slow and constant mode, to a vigorously stirred ethanolic solution containing oxalic acid (20 wt.% in excess with respect to the stoichiometric amount necessary to precipitate the metal precursors) and the powdered zeolite in a weight ratio of 9:1 with respect to the final oxide composition of the methanol catalyst. The precipitate was stirred for 3 h, then aged overnight. The catalyst was filtered, dried at 110 °C for 16 h and then calcined at 350 °C for 4 h, according to the stepwise procedure elsewhere reported [43].

2.4. Catalysts characterization

2.4.1. X-rays fluorescence (XRF) measurements

The analytical composition of Cu based catalysts were determined by XRF measurements, using a Bruker AXS–S4 Explorer spectrometer, equipped with a Rhodium X-ray source (Rh anode and 75 μm Be-window), a LiF 220 crystal analyzer and a 0.12° divergence collimator. The analytical composition of the catalysts was expressed in percentage by weight of oxides.

Table 1
Chemical composition, textural and surface properties of the methanol catalysts.

Sample	CuO	ZnO	ZrO_2	SA [m^2/g][b]		S_{Cu}[c]	D_{Cu}[d]	d_{Cu}[e]
	[wt.%][a]			Calcined	Reduced	[m^2/g]	[%]	[Å]
IT-OX/1	28.0	28.6	43.4	161	158	17	12.0	85
IT-OX/3	40.0	13.1	46.9	159	154	24	10.8	95
IT-OX/6	56.8	27.7	15.5	162	145	28	9.5	110

[a] From XRF measurements.
[b] Surface area B.E.T. from N_2 ads/des isotherms.
[c] Cu surface area from N_2O chemisorption measurements.
[d] Cu dispersion from N_2O chemisorption measurements.
[e] Cu average particle size: $d_{Cu} = 104/D_{Cu}(\%)$.

2.4.2. Total surface area (SA_{BET}) measurements

The textural properties of catalysts were determined by physical adsorption measurements of nitrogen to its boiling point (−196 °C), using a Micromeritics ASAP 2020 gas adsorption device. The isotherms were elaborated for assessment of surface area (SA) and porosity (PV), with the micropore volume (V_{micro}) determined by the *t*-plot approach.

2.4.3. X-Rays diffraction (XRD) measurements

XRD patterns of catalysts were obtained by a Philips X-Pert diffractometer operating at 40 kV and 30 mA, employing the Ni β-filtered Cu Kα radiation (λ = 1.5406 Å) in the 2θ range 10–80°. Identification of XRD patterns was made on the basis of the JCPDS database, while the metal particle size was determined by Scherrer equation assuming a Gaussian shape of the peaks.

2.4.4. Thermo-gravimetric analysis

Thermal analysis (DTG-60, Shimadzu) between 25 °C and 850 °C (10 °C/min) was carried out aiming to evaluate the thermal stability of the synthesized zeolites and to estimate the loss both of water and of organic molecules used as structure-directing agents (SDA).

2.4.5. Chemical composition and SEM analysis

SEM-EDAX analysis was carried out to study the morphology both of the crystalline phase of the MFI zeolites (FEI model Inspect) and of the hybrid catalysts (Philips XL-30-FEG) as well as to analyze the atomic composition on the examined surface (EDAX, Oxford 6587). The aluminum content of the zeolite structures was also verified by ICP-MS (PerkinElmer DRC -e).

2.4.6. Transmission electron microscopy (TEM) analysis

A Philips CM12 instrument equipped with a high-resolution camera was used to acquire and elaborate TEM images. Powdered samples were dispersed in 2-propanol under ultrasound irradiation and the resulting suspension put drop-wise on a holey carbon-coated support grid.

2.4.7. Temperature programmed reduction (TPR) measurements

The measurements of reducibility were performed in hydrogen atmosphere using a linear quartz micro-reactor (*i.d.*, 4 mm) fed with a 5 vol.% H_2/Ar at the flow rate of 30 *STP* mL/min. The experiments were carried out in the range 0–900 °C with a heating rate of 20 °C/min. The hydrogen consumption was monitored by a thermal conductivity detector (TCD), previously calibrated with a known amount of a commercial CuO standard. TPR data resulted very reproducible both in the maximum position (±3 K) and extent of H_2 consumption (±3%).

2.4.8. N_2O titration measurements

Copper surface area (S_{Cu}) and dispersion (D_{Cu}) values were obtained by "single-pulse" N_2O-titration measurements at 90 °C [44]. Before measurements the samples were reduced in situ at 300 °C in flowing H_2 (100 *STP* mL/min) for 1 h, then "flushed" at 583 K in nitrogen carrier flow (15 min) and further cooled down at 90 °C. S_{Cu} and D_{Cu} values were calculated assuming a Cu:N_2O = 2:1 titration stoichiometry and a surface atomic density of 1.46×10^{19} Cu_{at}/m^2, while, assuming a spherical shape, the Cu average particle size (d_{Cu}) was obtained from the conventional formula [44]: d_{Cu} (nm) = $104/D_{Cu}$ (%).

2.4.9. Temperature programmed desorption of NH_3 (NH_3-TPD)

NH_3-TPD measurements for the surface acidity determination were performed by using 100 mg of sample in a linear quartz micro-reactor (i.d., 4 mm; l., 200 mm), with a helium carrier flow of 25 *STP* mL/min. The experiments were carried out in the range 100–700 °C with a heating rate of 10 °C/min. The ammonia desorption was monitored by TCD, calibrated by the peak area of known pulses of NH_3. Prior of each measurements, the sample was pretreated at 300 °C with hydrogen flowing at 100 mL/min for 1 h and then cooled down to 150 °C and saturated at a flow rate of 25 mL/min for 1.5 h with a 5 vol.% NH_3/He stream. Then, the samples were purged in He atmosphere for ca. 1 h until a constant TCD level was obtained.

2.5. Catalytic tests

2.5.1. MeOH-to-DME dehydration reaction

Catalytic tests for the MeOH-to-DME dehydration reaction were performed in an experimental apparatus described elsewhere [45]. In order to evaluate the effect of temperature and catalyst acidity, the MFI samples were tested in the temperature range 140–200 °C, loading 150 mg of catalysts (pellets size: 300–500 μm) in each run. A flow of nitrogen carrier was saturated with pure methanol through a bubbler kept at 3.5 °C by a thermostatic bath (Julabo F12-ED, USA), to get a MeOH vapor pressure of 0.048 atm at a weight hourly space velocity (*WGSV*) of 2 g_{MeOH}/g_{cat}/h and a MeOH:N_2 volume ratio equal to 1:21.

In order to check the effect of water on the catalytic activity, according to literature procedure [46], in a different series of experiments the feed composition was changed by adding water in a ratio 1:10 with methanol but keeping the same reactant concentration (methanol:water:nitrogen = 1.0:0.2:21.0). This allowed comparing the effect of water on the DME production avoiding the effect of any change in reactant concentration.

Table 2
Chemical porosimetric and thermal properties of zeolite catalysts.

Sample	Si/Al_{gel}[a] [mol/mol]	Si/Al_{bulk}[a] [mol/mol]	SA[b] [m^2/g]	MV[c] [cm^3/g]	% Total Loss[d] (25–550 °C)	% Loss of water[d] (25–300 °C)	% Loss of Template[d] (300–550 °C)
MFI(15)	15	27	360	0.098	12.2	2.8	9.4
MFI(25)	25	38	365	0.084	12.5	2.6	9.9
MFI(50)	50	68	316	0.140	12.9	2.1	10.8
MFI(100)	100	127	382	0.094	13.0	1.4	11.6

[a] From ICP-MS measurements.
[b] Surface area B.E.T. from N_2 ads/des isotherms.
[c] Micropore volume from N_2 ads/des isotherms.
[d] From TG analysis.

Before of each test, the catalyst sample was conditioned under nitrogen flow at 200 °C for 3 h and the product stream composition was analyzed by gas chromatography (GC Agilent 7890A), equipped with a capillary column (J&W 125-1032) connected to a flame ionization detector.

2.5.2. CO_2 hydrogenation into MeOH or DME

The catalytic activity was investigated in a fixed-bed stainless steel reactor (i.d., 4 mm; l., 200 mm) at temperature ranging from 180 to 240 °C and a total pressure of 3.0 MPa (GHSV = 10,000 h^{-1}; CO_2:H_2:N_2 = 3:9:1). Prior to each test, the catalyst was reduced in situ at 300 °C for 1 h in pure hydrogen flow at atmospheric pressure. The reaction stream was analyzed by a GC equipped with a two-column separation system connected to a flame ionized detector (FID) and thermal conductivity detector (TCD), respectively. Conversion-selectivity data were calculated by both internal standard and mass-balance methods [26], each data set being obtained, with an accuracy of ±3%, from an average of three independent measurements.

3. Results and discussion

3.1. Physico-chemical properties of CuZnZr catalysts

Differently from the conventional coprecipitation of metal precursors by sodium or potassium carbonate/bicarbonate in aqueous solution to prepare Cu-based systems [44,47–51], the coprecipitation by oxalic acid in ethanol (gel-oxalate coprecipitation) represents a simple and fast procedure to obtain catalysts free of alkaline contamination [52]. The list of the methanol CuZnZr samples (IT-OX), along with the respective chemical composition and results of physico-chemical characterization, according to the aforementioned procedures, is reported in Table 1.

Although high loading of copper (50–70 wt.%) are generally used in methanol synthesis processes [51,53–56], three ternary catalysts were prepared with CuO concentration ranging from ca. 30 (IT-OX/1) to 60 wt.% (IT-OX/6). Surface characterization data point out that the gel-oxalate coprecipitation method is helpful for the obtainment of a large total surface area exposure (SA, 159–162 m^2/g), without any significant shrinkage upon reduction ($\Delta SA \leq 10$ %). In particular, the progressive decreasing of copper content (which corresponds to a higher cumulative concentration of zinc and zirconium oxides), accounts for a minor loss of surface area in the reduced samples, as the result of a reduced tendency to metal sintering. So, within the range of compositions investigated, the increase of copper surface area (S_{Cu}, 17 → 28 m^2_{Cu}/g) with copper loading does not significantly affect the metal dispersion (D_{Cu}, 12.0 → 9.5%), but the average size of the copper particles grows (d_{Cu}, 85 → 110 Å).

In order to evaluate the influence of the catalyst composition on the reduction kinetics of the various samples, H_2-TPR measurements were carried out. The profiles (see Fig. S1 in Supplementary section) display for all the IT-OX samples a main H_2 consumption peak centered at 248–262 °C (see also Table S1 in Supplementary section), shouldered on the left side of the main maximum and shifted to higher temperature with an increased copper loading. Such a peak is diagnostic of the reduction of CuO to metallic Cu below 300 °C, whereas the slight differences both in the onset reduction ($T_{o,red}$) and the maximum temperature (T_M) can be explained on the basis of the extent of copper-oxide(s) interaction, affected by the different chemical composition. A minor broad peak observed in the range of 300–700 °C was associated with an ongoing reduction of the ZnO promoter [44], resulting more favored in the IT/OX-3 sample characterized by a lower loading of ZnO (13.1 wt.%) well dispersed in presence of a high concentration of ZrO_2. In terms of reducibility, the IT-OX/6 sample exhibits the highest total H_2 consumption (5.2 $mmol_{tot}/g_{cat}$), fully ascribable to the highest CuO concentration (56.8 wt.%), whereas the normalization of quantitative data in terms of copper loading does not allow to evidence significant differences, since the ratio between the amount of H_2 consumed and the amount of reducible copper oxide contained in each sample was similar (H_2/Cu ≈ 0.90) in the temperature range 0–300 °C.

In order to obtain information on the crystalline phases present on the samples reduced at 300 °C under H_2 atmosphere, diffraction spectra were collected by XRD measurements (see Fig. S2 in Supplementary section). For all the samples, the main peaks are observable at 2θ values of 43.2 and 50.4, associated to metallic copper (JCPDS 01-089-2838), being indexed to (1 1 1) and (2 0 0) diffraction planes, respectively. The other diffraction peaks match the standard data for a hexagonal ZnO wurtzite (JCPDS 36-1451), with minor intense lines in the IT-OX/3 sample at lower ZnO content. On the whole, the samples appear completely reduced to metallic Cu without any evident detection of Cu_2O or CuO phases, also showing that the experimental variables during preparation have not visibly altered the main crystalline phases of the samples.

3.2. Physico-chemical properties of the MFI zeolites

Physico–chemical properties and quantitative data of TG analysis of the as-made MFI zeolites are summarized in Table 2.

Despite a high degree of crystallinity exhibited by all the samples (see Fig. S3 in Supplementary section), the increase of the molar Si/Al bulk ratio proves that not all the aluminum added to synthesis gel is incorporated in the catalyst [57]. From thermograms (Fig. S4 in Supplementary section), it is also possible to observe two main exothermic peaks related to template oxidation, at lower (ca. 420 °C) and at higher (ca. 480 °C) temperature, respectively. The first appears more prominent than the latter when aluminum content decreases, due to a reduction of number and strength of acid sites at which the SDA molecule is bonded. Moreover, from Table 2 it clearly appears the decrease of water content with increasing of Si/Al ratio due to an increase of hydrophobicity of zeolite, whilst SDA content decreases with increasing of Al content [57].

Scanning electron microscopy, reported in Fig. 1, shows a crystals size of about 5 μm, with the classical shape of MFI structure depending on the aluminum content and varying from prismatic to spherical shape as the metal content decreases [58].

Table 3
Quantitative data of NH_3-TPD and acid sites distribution.

Sample	NH_3-uptake [μmol/g_{cat}]	T_{d1} [a] [°C]	x_1 [b]	T_{d2} [c] [°C]	x_2 [d]	R^2
MFI(15)	602	213	0.45	406	0.55	0.988
MFI(25)	515	210	0.42	399	0.58	0.993
MFI(50)	354	195	0.45	396	0.55	0.994
MFI(100)	147	189	0.46	355	0.54	0.990

[a] Temperature of maximum desorption of NH_3 between 100 and 300 °C.
[b] Fractional population of sites between 100 and 300 °C.
[c] Temperature of maximum desorption of NH_3 between 300 and 500 °C.
[d] Fractional population of sites between 300 and 500 °C.

Table 4
Catalytic testing in direct CO_2-to-DME hydrogenation reaction (T_R, 240 °C; CO_2:H_2:N_2, 3:9:1).

Run	Sample	P_R [MPa]	*GHSV* [*NL*/kg_{cat}/h]	X_{CO2} [%]	S_{DME} [%]	S_{MeOH} [%]	S_{CO} [%]	Y_{DME} [%]
1	UNIT-25/9-OX	3.0	10,000	15.9	38.5	9.9	51.6	6.1
2	UNIT-25/9-OX	3.0	2,500	19.3	44.6	10.5	44.9	8.6
3	UNIT-25/9-OX	5.0	2,500	23.6	49.3	25.5	24.5	11.6

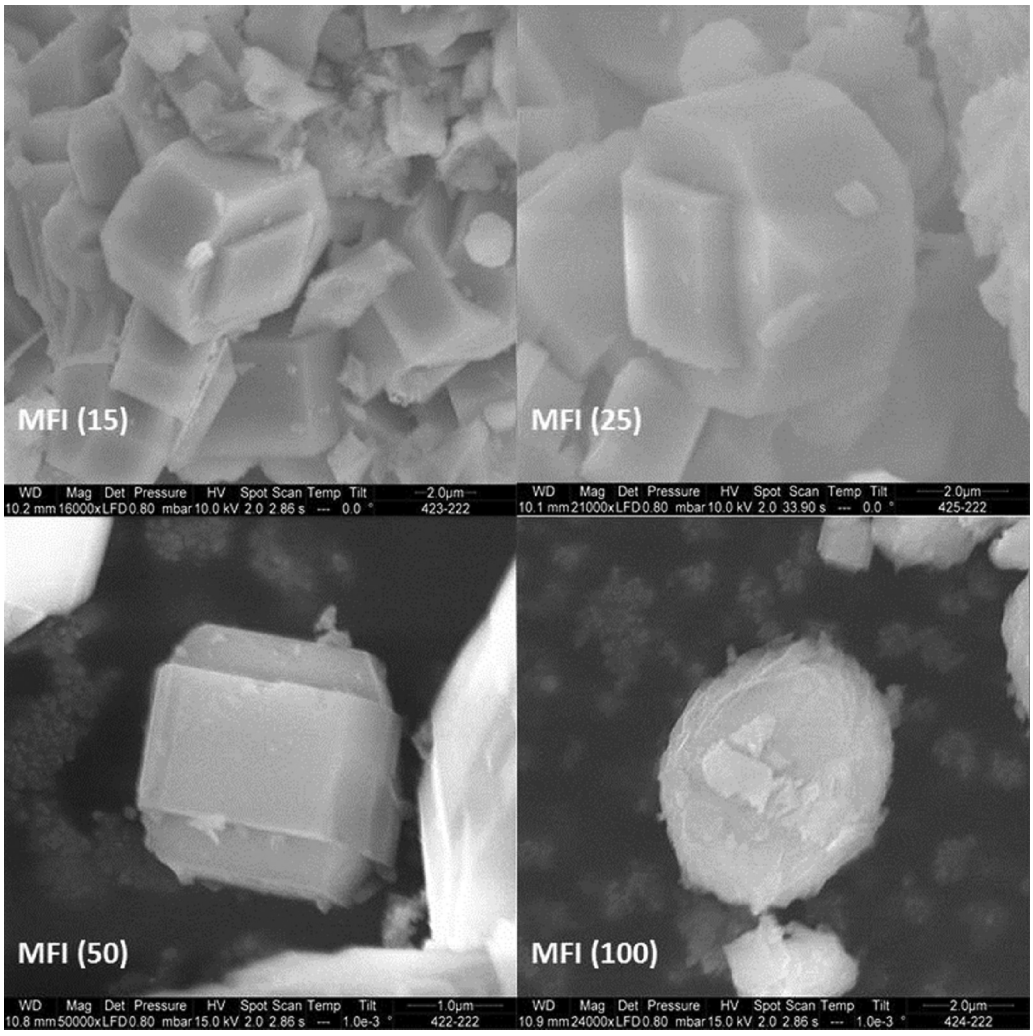

Fig. 1. SEM analysis of the H-MFI crystals.

The NH_3-TPD profiles of the studied MFI-type zeolites (see Fig. S5-A in Supplementary section) display two main peaks, reflecting the interaction of ammonia with weak and strong acid sites, at low (150–250 °C) and high temperature (350–450 °C), respectively [59,60]. Although by NH_3-TPD measurements is not possible to discriminate between Brønsted and Lewis acidity, the interpretation of weaker sorption causing a low-temperature TPD peak is generally associated either to the presence of Lewis acid sites on zeolite framework sites or to extra-framework aluminum oxide/hydroxide species [61,62], also eliminable by long flushing times [63,64] or steam treatment prior to adsorption [65]. Instead, the peak at higher temperature is usually associated to Brønsted acid sites, generated by framework Al ions [66]. In quantitative terms, Table 3 reports the overall NH_3-uptake for each sample, which repre-

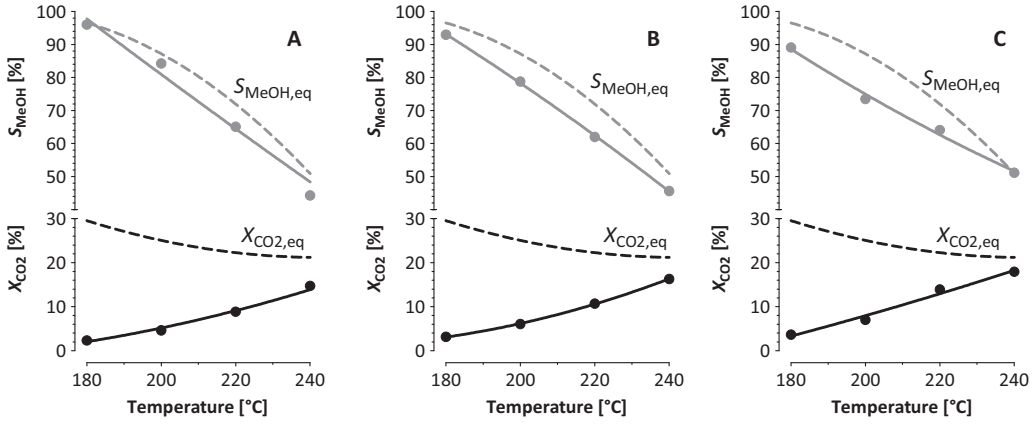

Fig. 2. CO_2 conversion and MeOH selectivity (continuous lines) in the range of 180–240 °C of (A) IT-OX/1, (B) IT-OX/3 and (C) IT-OX/6 catalysts (experimental conditions: P_R, 3.0 MPa; *GHSV*, 10,000 *NTP* mL/g_{cat}/h; CO_2:H_2:N_2, 9:3:1). Dotted lines refer to equilibrium values (determined as described in Appendix A of the Supplementary section).

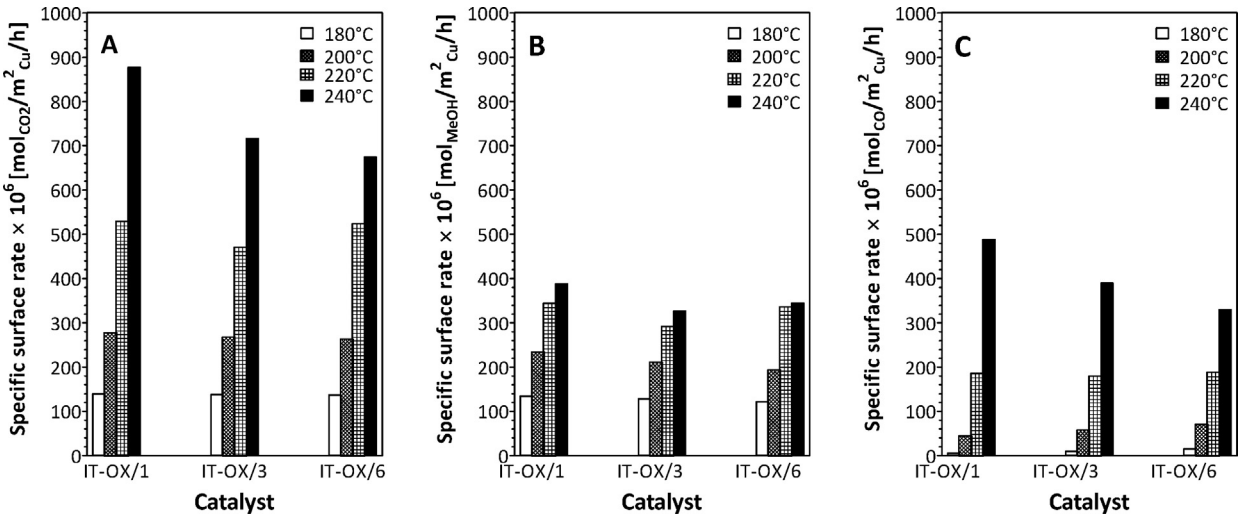

Fig. 3. Specific surface rate of (A) CO_2 conversion, (B) MeOH and (C) CO formation (P_R, 3.0 MPa; *GHSV*, 10,000 *NTP* mL/g_{cat}/h; CO_2:H_2:N_2, 9:3:1).

sents the total amount of acidic sites, and the relative population of weak and strong sites at low and high temperature, respectively. Although all the samples disclose a similar fraction of weak (0.42–0.46) and strong sites (0.54–0.58), with an uptake of 602 $\mu mol_{NH3}/g_{cat}$, the MFI(15) zeolite shows the highest number of acid sites, whereas the MFI(100) exhibits the lowest amount of NH_3-release in the temperature range considered, so drawing the following scale of acidity:

MFI(15) > MFI(25) > MFI(50) > MFI(100)

As a rule, this acidity scale linearly follows the Si/Al ratio, with a lower ratio corresponding to a higher acidity (see Fig. S5-B in Supplemetary Section). It is evident that a decrease of Si/Al ratio (higher acidity) also matches an increase of temperature of maxima desorption (T_d, see Table 3), not imputable to stronger acid sites but to a higher NH_3 coverage.

3.3. *Catalytic testing of CuZnZr catalysts in CO_2-to-MeOH hydrogenation reaction*

The catalytic performance of the ternary CuZnZr catalysts was preliminary assessed in the CO_2-to-MeOH hydrogenation reaction, at reaction temperature ranging from 180 to 240 °C, pressure 3.0 MPa and space velocity of 10,000 h^{-1}. The results of the catalytic tests, shown in Fig. 2, reveal that the carbon-containing products

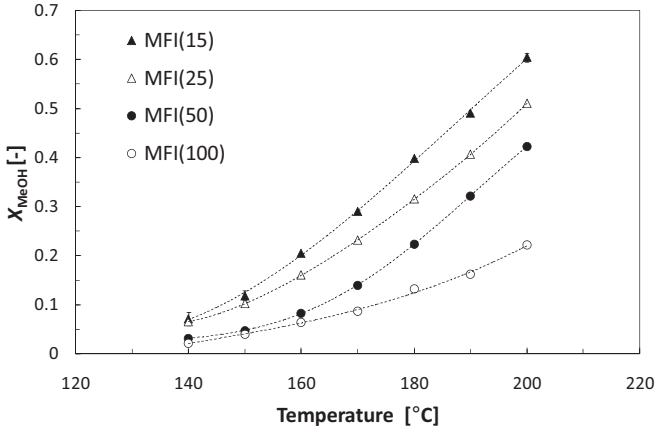

Fig. 4. Methanol conversion to DME over different MFI samples (P_R, 0.1 MPa; *WGSV*, 2 g_{MeOH}/g_{cat}/h; MeOH:N_2, 1:21).

detected were methanol and carbon monoxide only. As a general rule, it can be observed that the conversion of CO_2 increases with reaction temperature, while the MeOH selectivity gradually decreases. In particular, in the temperature range investigated, the IT-OX/1 sample (Fig. 2A) exhibits X_{CO2} values raising from 2.3 (180 °C) to 14.7 % (240 °C), while S_{MeOH} correspondingly decreases from 96.0 to 44.3%. A similar activity–selectivity pattern is displayed by the IT-OX/3 sample (Fig. 2B) showing a slightly higher CO_2 conversion, while the IT-OX/6 sample (Fig. 2C) attains higher X_{CO2} and S_{MeOH} values, very close to equilibrium at 240 °C (X_{CO2}, 18.0%; S_{MeOH}, 51.1%).

In principle, the differences observed in the catalytic behavior of the samples could be ascribable to the different copper content, also mirroring a different extent of metal surface area (S_{Cu}, see Table 1).

Really, as shown in Fig. 3, that appears true until 200 °C, since the specific surface rate of CO_2 conversion (Fig. 3A) remains almost unchanged for all the investigated samples (ca. 270 $\mu mol_{CO2}/m^2_{Cu}$/h). Instead, at higher reaction temperature (i.e., 240 °C), the specific surface rate of CO_2 conversion significantly changes, reaching with IT-OX/1 a maximum value of 880 $\mu mol_{CO2}/m^2_{Cu}$/h and a minimum of 670 $\mu mol_{CO2}/m^2_{Cu}$/h with IT-OX/6. Moreover, by looking at the surface rate of product formation (Figs. 3B and 3C), it clearly appears that the surface properties of the catalysts mainly affect the rate of CO formation. In fact, by increasing the reaction temperature, the rate of MeOH formation progressively increases for all the samples (see Fig. 3B), although above 220 °C no visible enhancement can be observed, with the values becoming leveled near 240 °C (360–390 $\mu mol_{MeOH}/m^2_{Cu}$/h). On the contrary, the rate of CO formation (see Fig. 3C) remains low enough until 220 °C (ca. 185 $\mu mol_{CO}/m^2_{Cu}$/h), whereas at higher temperature a net increase is recorded for all the samples, being the side reactions, RWGS (3) and MeOH-to-CO decomposition (4), more favored than the CO_2-to-MeOH hydrogenation Reaction (1). In particular, at 240 °C, the IT-OX/1 catalyst shows the highest rate of CO formation (470 $\mu mol_{CO}/m^2_{Cu}$/h), much higher than that observed for IT-OX/3 (390 $\mu mol_{CO}/m^2_{Cu}$/h) and IT-OX/6 (320 $\mu mol_{CO}/m^2_{Cu}$/h), demonstrating a structure-sensitive trend directly referable to the copper dispersion. Likely, as the reaction proceeds, the formation of water should be responsible for a partial oxidation of Cu^0 sites to $Cu^{\delta+}$ sites [2,67], at higher rate on smaller copper particles (i.e., IT-OX/1, see Table 1) on which the formation of CO (at expenses of MeOH) is favored [26,68]. These findings confirm once again that the catalytic performance of the CuZnZr systems in CO_2-to-MeOH hydrogenation reaction cannot

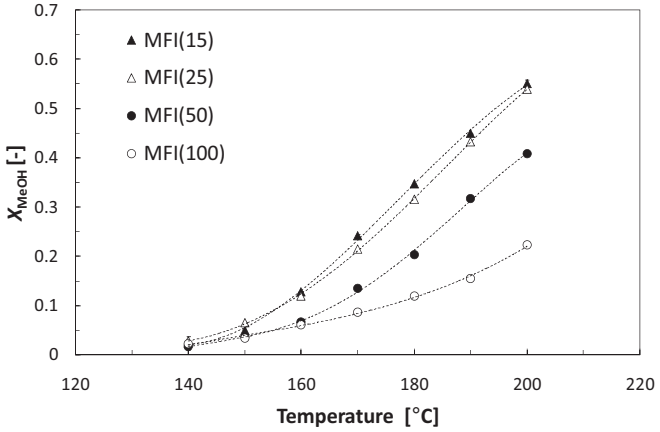

Fig. 5. Zeolites activity in MeOH-to-DME dehydration reaction. Effect of water in the feed (P_R, 0.1 MPa; *WGSV*, 2 g_{MeOH}/g_{cat}/h; MeOH:H_2O:N_2, 1.0:0.2:21.0).

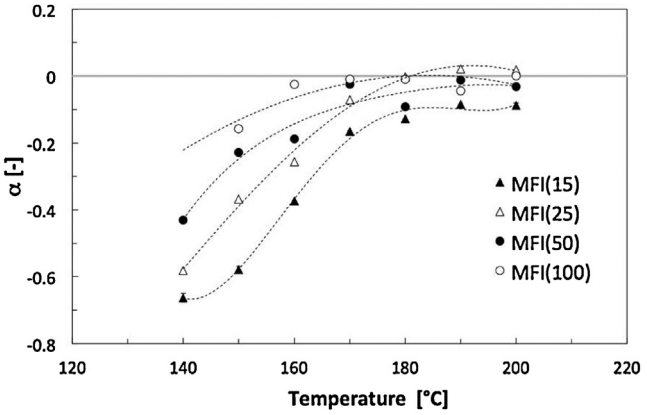

Fig. 6. Effect of water over methanol conversion. Fractionary loss (α) in conversion.

be merely related to the availability of metallic sites (Cu^0). In fact, considering the complex nature of the reaction pathway [69–71], the occurrence of a very intimate contact between metallic copper and oxide carriers [68], the stabilization of copper species of low-valence ($Cu^{\delta+}$) onto oxygen surface vacancies [71] or a change in the morphology of the metallic sites [41,72] are also determinant to ensure high methanol selectivity [52].

On the basis of the above results, the IT-OX/6 catalyst was chosen as a reference composition to develop a multifunctional CuZnZr-zeolite system. In fact, considering that the operative temperature for the direct DME synthesis by CO_2 hydrogenation is above 200 °C [27], the selected composition should ensure good activity in CO_2 activation, with high MeOH selectivity and limited CO formation.

3.4. Methanol dehydration catalytic tests

Prior to assessing the catalytic behavior of the hybrid catalysts in the direct DME synthesis, the zeolites were evaluated in the MeOH-to-DME dehydration reaction. In Fig. 4 the methanol conversion X_{MeOH} for all the tested MFI samples is reported. It is noteworthy that DME was the only detected product, keeping the catalyst selectivity close to 1 in the investigated temperature range. As the effect of temperature is considered, the reaction proceeds more when increasing temperature. Also the decrease of the Si/Al ratio promotes the methanol conversion, confirming that, for moderate acid catalyst, the more acid is the zeolite the better it catalyzes the reaction [73], avoiding any secondary reaction leading to either olefins or heaviest compounds such as polymethylbenzenes also acting as coke precursors [74].

When the effect of water addition is considered, the conversion data are reported in Fig. 5. When comparing with the water-free data, it clearly appears that the catalytic effect decrease at any Si/Al ratio but the activity order does not change according to the zeolite acidity. Nevertheless, in order to compare the water effect the fractional drop in methanol conversion α can be calculated as it follows:

$$\alpha = \frac{X^*_{MeOH} - X_{MeOH}}{X_{MeOH}}$$

where X^*_{MeOH} is the methanol conversion in presence of water, measured in the same process and catalyst condition of the water-free conversion X_{MeOH}.

Data are shown in Fig. 6 and it clearly appears that no significant effect of water presence was observed above 180 °C, since the α drop is always lower than 0.1.

Therefore, it is suggested that when temperature conditions higher than 180 °C the water presence does not affect the acid catalyst performance. On the contrary, at temperatures below 180 °C, it clearly appears that the catalyst activity is affected by the water presence according to its acidity. In fact, the lower the Si/Al ratio, the greater the α drop, decreasing the methanol conversion up to 70% at low temperature for MFI(15), being the most acid sample. It is also interesting to point out that the water does not have any practical effect on methanol conversion for the MFI(100), the sample exhibiting a lower acidity.

On the basis of the obtained results, the MFI(25) zeolite was selected to be combined with the methanol catalysts for the direct CO_2-to-DME hydrogenation reaction, representing the best compromise between catalytic activity and resistance to deactivation in presence of water.

3.5. Catalytic performance of hybrid systems in direct CO_2-to-DME hydrogenation reaction

Initially, in order to study the influence of the zeolite acidity on the performance of the hybrid system, under conditions where the overall CO_2-to-DME hydrogenation process is controlled by the methanol synthesis rate on the CuZnZr catalyst, the methanol synthesis catalyst (IT-OX/6) and the MFI(25) zeolite were physically mixed starting from the pre-pelletized components in a CuZnZr:zeolite mass ratio of 1:1 (UNIT-25/1-PM) and 9:1 (UNIT-25/9-PM).

As shown in Fig. 7, despite a slightly higher selectivity to CO (S_{CO}), with a CO_2 conversion (X_{CO2}) of 15.4% and a DME selectivity (S_{DME}) of 37.6%, the UNIT-25/9-PM system exhibits a better performance than the UNIT-25/1-PM system (X_{CO2}, 11.8%; S_{DME}, 37.1%),

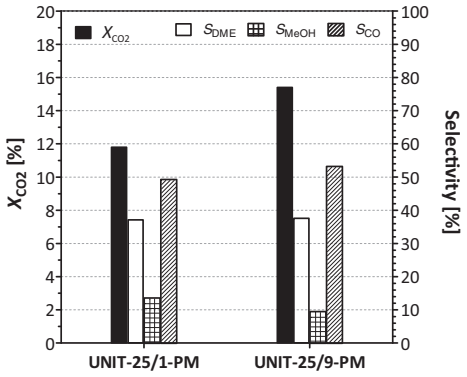

Fig. 7. Conversion of CO_2 and selectivity to DME, MeOH and CO over the hybrid mixed systems (T_R, 240 °C; P_R, 3.0 MPa, *GHSV*, 10,000 mL/g_{cat}/h; CO_2:H_2:N_2, 3:9:1).

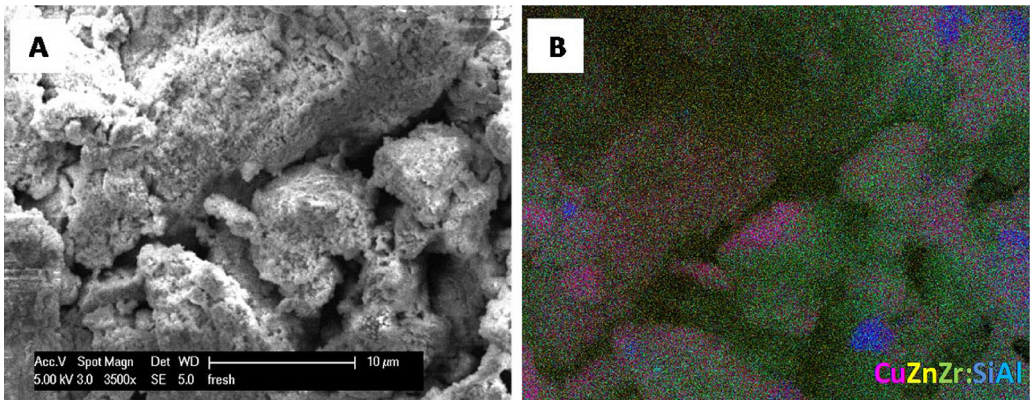

Fig. 8. SEM micrograph (A) and EDAX mapping (B) of the hybrid UNIT-25/9-OX catalyst.

demonstrating so that there is no need for a great number of acid sites (like in UNIT-25/1-PM) to perform the direct CO_2-to-DME hydrogenation reaction.

Then, considering that a metal-oxide/acid site ratio of 9:1 was enough to attain high DME productivity, a gel-oxalate coprecipitated hybrid catalyst (UNIT-25/9-OX) with a CuZnZr:zeolite composition of 9:1 was also prepared and tested for comparison in CO_2-to-DME hydrogenation reaction. In principle, the generation of a hybrid system by coprecipitation should account for a superior yield of DME (Y_{DME}), as the result of a long-range "homogeneity", especially in terms of sites distribution among metal-oxide and acid sites.

In Table 4 the catalytic data obtained in various experimental conditions are reported.

Really, with the coprecipitated UNIT-25/9-OX catalyst (Run 1), not only the CO_2 conversion is just higher than that obtained over the mixed system under the same conditions (X_{CO2}, 15.9% vs. 15.4%), but also methanol is more efficiently dehydrated to DME on the neighbouring acid sites, reaching a DME yield of 6.1% (against 5.8% of UNIT-25/9-PM). This value of DME yield obtained in the direct CO_2-to-DME hydrogenation reaction by a hybrid coprecipitated system is certainly very interesting; in fact, it is not demonstrated so far that a higher degree of interdispersion among the active components (as it should be in the case of hybrid coprecipitated systems in respect to the mixed systems) leads to better catalytic performance [14,17,28,]. Indeed, as shown in Fig. 8A, the hybrid catalyst presents a sponge-like structure, typical of porous systems, with a good morphological homogeneity, in terms of uniform distribution of elements per unit of surface (Fig. 8B). Evidently, the gel-oxalate coprecipitation of methanol synthesis precursors in a solution of dispersed zeolite favors a good mixing among the elements, also enhancing their distribution onto the zeolite framework.

These findings are well supported by TEM analysis (see Fig. 9), in which the hybrid catalyst appears to be characterized by Cu particles with size ranging from 10 to 35 nm surrounded by ZnO (filamentous particles), ZrO_2 (lighter particles of regular shape) and zeolite (particles with lamellar shape). By comparing the fresh and used catalysts, it does not emerge any substantial difference neither in terms of dispersion of Cu particles nor in the distribution of ZnO and ZrO_2 particles. In the used sample, the zeolite continues to be present with a random distribution.

However, contrarily to what expected, neither by using the mixed systems (even at different CuZnZr:zeolite weight ratio) nor the hybrid coprecipitated catalyst, the conversion of CO_2 benefited the presence of the acid sites that were supposed to shift positively the equilibrium giving CO_2 conversion values higher than those obtained in CO_2-to-MeOH hydrogenation reaction under the same experimental conditions (X_{CO2}, 18.0%; see Section 3.3). That can be explained by a higher accumulation of water in the catalytic bed reactor during the DME production process, so preventing the conversion of CO_2 to be enhanced.

Anyhow, in the attempt to further increase the DME yield, the catalytic behavior of the coprecipitated hybrid system was also evaluated at lower gas hourly space velocity (Run 2). Thus, when the *GHSV* was as low as 2500 $NL/kg_{cat}/h$, a net increase of CO_2 conversion (19.3%) was recorded, followed by a higher DME selectivity (44.6%), in detriment of the CO selectivity (44.9%). Indeed, by decreasing the space velocity, the contact time of the CO_2–H_2 mixture over the catalyst surface is increased, leading to higher driving force for CO_2 conversion. Moreover, the increase of DME selectivity at lower space velocity is also associable to an increase of the contact time. In fact, by increasing the contact time, the methanol dehydration reaction will proceed to completion and the DME selectivity will result to be increased.

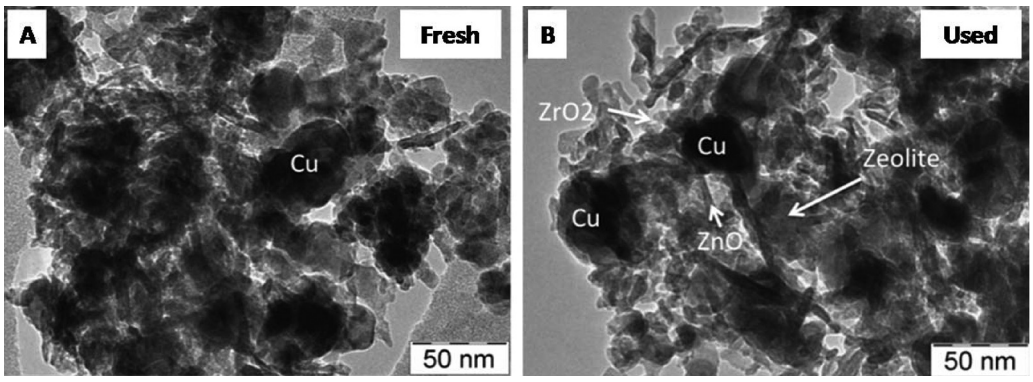

Fig. 9. TEM images of the UNIT-25/9-OX catalyst: (A) fresh sample; (B) used sample (T_R, 240 °C; P_R, 3.0 MPa; *GHSV*: 10,000 *NL*/kgcat/h; CO_2:H_2:N_2, 3:9:1).

At last, by holding constant temperature (240 °C) and space velocity (2500 *N*L/kg$_{cat}$/h), an experiment was carried out at a reaction pressure of 5.0 MPa by using the UNIT-25/9-OX catalyst. The results obtained (Run 3) show that the conversion of CO_2 significantly increases up to 23.6%. Furthermore, under these conditions, a remarkable decreasing of CO selectivity was observed (S_{CO}, 24.5%), so implying higher selectivity values both to MeOH (25.5%) and DME (49.3%). This result suggests that an adjustment of the operative conditions can allow to improve the catalytic behavior of the hybrid coprecipitated system, further enhancing the DME productivity.

4. Conclusions

Independent measurements both on CuZnZr catalysts for CO_2-to-MeOH hydrogenation reaction and on H-MFI type zeolites in MeOH-to-DME dehydration reaction allowed to shed light on the factors controlling the single steps of the synthesis of DME from CO_2–H_2 mixtures.

Not only the choice of the preparation method plays a crucial role to ensure suitable textural and surface properties of Cu-Zn-Zr catalysts, but also the chemical composition must be carefully selected in order to maximize the amount of CO_2 and H_2 activation sites at the metal-oxide interface. In this context, the gel-oxalate coprecipitation of the methanol precursors with a Cu loading as high as 57 wt.% allowed to achieve high CO_2 conversion levels, coupled to high MeOH selectivity and limited CO formation.

In the MeOH dehydration reaction, the Si/Al ratio of zeolite must be carefully tuned, as it significantly affects acidity as well as MeOH conversion and selectivity to DME or higher hydrocarbons. On the basis of the results obtained in presence and in absence of water, a Si/Al ratio of 38 was the best compromise between catalytic activity and resistance to deactivation by water.

Multifunctional CuZnZr-zeolite systems prepared by combination of the selected methanol synthesis (CuZnZr) and methanol dehydration (H-MFI) catalysts resulted to be effective to produce DME by CO_2 hydrogenation in one step. With respect to the conventional physical mixing between methanol catalyst and zeolite, the incorporation of metal-oxide and acid sites in a single system can enhance the CO_2 conversion, also allowing a higher rate of MeOH formation/dehydration on neighbouring surface sites (DME yield of 11.6% at 5.0 MPa, 240 °C and 2500 *N*L/kg$_{cat}$/h). The homogeneous distribution of metal-oxide-acid sites interacting among them was claimed as responsible for this superior behavior.

Acknowledgements

This work was financially supported through the project "BIO4BIO – Biomolecular and Energy valorization of residual biomass from Agroindustry and Fishing Industry" led by the Cluster Sicily Agrobio and Fishing Industry and funded by the Italian Research Fund (PON R&C 2007–2013, DD 713/Ric. – PON02 00451 3362376).

Appendix A. Supplementary data

Supplementary data associated with this article can be found, in the online version, at http://dx.doi.org/10.1016/j.apcatb.2015.04.032.

References

[1] G. Centi, S. Perathoner, Catal. Today 148 (2009) 191–205.
[2] X. An, Y.Z. Zuo, Q. Zhang, D.Z. Wang, J.F. Wang, Ind. Eng. Chem. Res. 47 (2008) 6547–6554.
[3] Q. Zhang, Y.Z. Zuo, M.H. Han, J.F. Wang, Y. Jin, F. Wei, Catal. Today 150 (2010) 55–60.
[4] A.A. Khozema, A.Z. Ahmad, M.R. Abdul, Renew. Sustain. Energy Rev. 44 (2015) 508–518.
[5] M. Xu, J.H. Lunsford, D.W. Goodman, A. Bhattacharyya, Appl. Catal. A: Gen. 149 (1997) 289–301.
[6] F. Frusteri, L. Spadaro, O. Di Blasi, G. Bonura, F. Arena, Eur. Automob. Eng. Coop. — 10th EAEC Eur. Automot. Congr. 2 (2005) 588–599.
[7] C. Arcoumanis, C. Bae, R. Crookes, E. Kinoshita, Fuel 87 (2008) 1014–1030.
[8] M. Marchionna, R. Petrini, D. Sanfilippo, G. Migliavacca, Fuel Process. Technol. 89 (2008) 1255–1261.
[9] T.A. Semelsberger, R.L. Borup, H.L. Greene, J. Power, Sources 156 (2006) 497–511.
[10] Y. Zhu, S. Wang, X. Ge, Q. Liu, Z. Luo, K. Cen, Fuel Process. Technol. 91 (2010) 424–429.
[11] J.W. Bae, S.H. Kang, Y.J. Lee, K.W. Jun, J. Ind. Eng. Chem. 15 (2009) 566–572.
[12] L.A. Pellegrini, G. Soave, S. Gamba, S. Lange, Appl. Energy 88 (2011) 4891–4897.
[13] G. Jia, Y. Tan, Y. Han, Ind. Eng. Chem. Res. 45 (2006) 1152–1159.
[14] S.P. Naik, H. Du, H. Wan, V. Bui, J.D. Miller, W.W. Zmierczak, Ind. Eng. Chem. Res. 47 (2008) 9791–9794.
[15] J. Ma, N. Sun, X. Zhang, N. Zhao, F. Xiao, W. Wei, et al., Catal. Today 148 (2009) 221–231.
[16] G.A. Olah, Angew. Chem. Int. Ed. 52 (2013) 104–107.
[17] G. Bonura, M. Cordaro, L. Spadaro, C. Cannilla, F. Arena, F. Frusteri, Appl. Catal. B: Environ. 140–141 (2013) 16–24.
[18] Y.-N. Li, R. Ma, L.-N. He, Z.-F. Diao, Catal. Sci. Technol. 4 (2014) 1498–1512.
[19] Y. Zhang, D. Li, S. Zhang, K. Wang, J. Wu, RSC Adv. 4 (2014) 16391–16396.
[20] G.A. Olah, A. Goeppert, G.K. Surya Prakash, J. Org. Chem. 74 (2009) 487–498.
[21] W.-H. Chen, B.-J. Lin, H.-M. Lee, M.-H. Huang, Appl. Energy 98 (2012) 92–101.
[22] F. Arena, L. Spadaro, O. Di Blasi, G. Bonura, F. Frusteri, Stud. Surf. Sci. Catal. 147 (2004) 385–390.
[23] R.-W. Liu, Z.-Z. Qin, H.-B. Ji, T.-M. Su, Ind. Eng. Chem. Res. 52 (2013) 16648–16655.
[24] M.-H. Zhang, Z.-M. Liu, G.-D. Lin, H.-B. Zhang, Appl. Catal. A: Gen. 451 (2013) 28–35.
[25] G. Bonura, M. Cordaro, C. Cannilla, A. Mezzapica, L. Spadaro, F. Arena, F. Frusteri, Catal. Today 228 (2014) 51–57.
[26] F. Frusteri, M. Cordaro, C. Cannilla, G. Bonura, Appl. Catal. B: Environ. 162 (2015) 57–65.
[27] A. García-Trenco, A. Martínez, Appl. Catal. A: Gen. 411–412 (2012) 170–179.
[28] A. García-Trenco, S. Valencia, A. Martínez, Appl. Catal. A: Gen. 468 (2013) 102–111.
[29] O. Oyola-Rivera, M.A. Baltanás, N. Cardona-Martínez, J. CO_2 Util. 9 (2015) 8–15.
[30] A.T. Aguayo, J. Ereña, D. Mier, J.M. Arandes, M. Olazar, J. Bilbao, Ind. Eng. Chem. Res. 46 (2007) 5522–5530.
[31] S. Allahyari, M. Haghighi, A. Ebadi, S. Hosseinzadeh, Energy Convers. Manage. 83 (2014) 212–222.
[32] J. Ereña, R. Garoña, J.M. Arandes, A.T. Aguayo, J. Bilbao, Catal. Today 107–108 (2005) 467–473.
[33] W. Gao, H. Wang, Y. Wang, W. Guo, M. Jia, J. Rare Earths 31 (2013) 470–476.
[34] A. García-Trenco, A. Vidal-Moya, A. Martínez, Catal. Today 179 (2012) 43–51.
[35] R. Khoshbin, M. Haghighi, Chem. Eng. Res. Des. 91 (2013) 1111–1122.
[36] I. Sierra, J. Ereña, A.T. Aguayo, J.M. Arandes, M. Olazar, J. Bilbao, Appl. Catal. B: Environ. 106 (2011) 167–173.
[37] J.L. Li, X.G. Zhang, T. Inui, Appl. Catal. A: Gen. 147 (1996) 23–33.
[38] D. Mao, W. Yang, J. Xia, B. Zhang, G. Lu, J. Mol. Catal. A 250 (2006) 138–144.
[39] I. Sierra, J. Ereña, A.T. Aguayo, J.M. Arandes, J. Bilbao, Appl. Catal. B: Environ. 94 (2010) 108–116.
[40] J.W. Bae, S.-H. Kang, Y.-J. Lee, K.-W. Jun, Appl. Catal. B: Environ. 90 (2009) 426–435.
[41] G. Bonura, M. Cordaro, C. Cannilla, F. Arena, F. Frusteri, Appl. Catal. B: Environ. 152–153 (2014) 152–161.
[42] M. Migliori, E. Catizzone, A. Aloise, G. Giordano, Ind. Eng. Chem. Res. 53 (2014) 14885–14891.
[43] Q. Sun, Y.L. Zhang, H.Y. Chen, J.F. Deng, D. Wu, S.Y. Chen, J. Catal. 167 (1997) 92–105.
[44] F. Arena, K. Barbera, G. Italiano, G. Bonura, L. Spadaro, F. Frusteri, J. Catal. 249 (2007) 185–194.
[45] M. Migliori, A. Aloise, G. Giordano, Catal. Today 227 (2014) 138–143.
[46] L. Vanoye, A. Favre-Réguillon, P. Munno, J.F. Rodríguez, S. Dupuy, S. Pallier, I. Pitault, C. De Bellefona, Catal. Today 215 (2013) 239–242.
[47] P. Kowalik, M. Konkol, M. Kondracka, W. Próchniak, R. Bicki, P. Wiercioch, Appl. Catal. A: Gen. 452 (2013) 139–146.
[48] R. Raudaskoski, M. Veringa Niemelä, R.L. Keiski, Top. Catal. 45 (2007) 57–60.
[49] R. Ladera, F.J. Pérez-Alonso, J.M. González-Carballo, M. Ojeda, S. Rojas, J.L.G. Fierro, Appl. Catal. B: Environ. 142–143 (2013) 241–248.
[50] H. Ahouari, A. Soualah, A. Le Valant, L. Pinard, P. Magnoux, Y. Pouilloux, React. Kinet. Mech. Catal. 110 (2013) 131–145.
[51] J. Słoczyński, R. Grabowski, P. Olszewski, A. Kozłowska, J. Stoch, M. Lachowska, J. Skrzypek, Appl. Catal. A: Gen. 310 (2006) 127–137.
[52] Y. Ma, Q. Sun, D. Wu, W.-H. Fan, Y.-L. Zhang, J.-F. Deng, Appl. Catal. A: Gen. 171 (1998) 45–55.
[53] C. Baltes, S. Vukojević, F. Schüth, J. Catal. 258 (2008) 334–344.
[54] I. Kasatkin, P. Kurr, B. Kniep, A. Trunschke, R. Schlögl, Angew. Chem. 119 (2007) 7465–7468.

[55] Y. Nitta, O. Suwata, Y. Ikeda, Y. Okamoto, T. Imanaka, Catal. Lett. 26 (1994) 345–354.
[56] P.J.A. Tijm, F.J. Waller, D.M. Brown, Appl. Catal. A 221 (2001) 275–282.
[57] M. Ali, B. Brisdon, W.J. Thomas, Appl. Catal. A: Gen. 252 (2003) 149–162.
[58] T. Armaroli, L.J. Simon, M. Digne, T. Montanari, M. Bevilacqua, V. Valtchev, J. Patarin, G. Busca, Appl. Catal. A: Gen. 306 (2006) 78–84.
[59] N. Katada, K. Suzuki, T. Noda, T. Sastre, M. Niwa, J. Phys. Chem. C 113 (2009) 19208–19217.
[60] F. Lónyi, J. Valyon, Micropor. Mater. 47 (2001) 293–301.
[61] A. Auroux, Top. Catal. 4 (1997) 71–89.
[62] G.L. Woolery, G.H. Kuehl, H.C. Timken, A.W. Chester, J.C. Vartuli, Zeolites 19 (1997) 288–296.
[63] L. Forni, F.P. Vatti, E. Ortoleva, Micropor. Mater. 3 (1995) 367–375.
[64] R.W. Weber, J.C.Q. Fletcher, K.P. Moller, C.T. O'Connor, Micropor. Mater. 7 (1996) 15–25.
[65] G. Bagnasco, J. Catal. 159 (1996) 249–252.
[66] D.J. Parrillo, C. Lee, R.J. Gorte, Appl. Catal. A 110 (1994) 67–74.
[67] F. Arena, G. Italiano, K. Barbera, S. Bordiga, G. Bonura, L. Spadaro, F. Frusteri, Appl. Catal. A 350 (2008) 16–23.
[68] I.A. Fisher, A.T. Bell, J. Catal. 172 (1997) 222–237.
[69] X.-M. Liu, G.Q. Lu, Z.-F. Yan, J. Beltramini, Ind. Eng. Chem. Res. 42 (2003) 6518–6530.
[70] F. Arena, G. Italiano, K. Barbera, G. Bonura, L. Spadaro, F. Frusteri, Catal. Today 143 (2009) 80–85.
[71] W. Wang, S. Wang, X. Ma, J. Gong, Chem. Soc. Rev. 40 (2011) 3703–3727.
[72] S.-I. Fujita, S. Moribe, Y. Kanamori, M. Kakudate, N. Takezawa, Appl. Catal. A 207 (2001) 121–128.
[73] H. Li, S. He, K. Ma, Q. Wu, Q. Jiao, K. Sun, Appl. Catal. A: Gen. 450 (2013) 152–159.
[74] M. Bjørgen, S. Svelle, F. Joensen, J. Nerlov, S. Kolboe, F. Bonino, L. Palumbo, S. Bordiga, U. Olsbye, J. Catal 249 (2007) 195–207.